Inclination dependence of planar film boiling stability

Eskil Aursand[a,*]

[a]*Department of Energy and Process Engineering, Norwegian University of Science and Technology (NTNU), Trondheim N-7491, Norway*

Abstract

Understanding the dynamics of film boiling is crucial for predicting its heat transfer properties. Besides the complete breakdown of film boiling (Leidenfrost point), the most prominent transition is the change from a steady state to an unstable and oscillating vapor film. Here we consider the stability of saturated planar non-horizontal film boiling, with particular attention given to its dependence on inclination angle. Based on the lubrication approximation and a quasi-equilibrium evaporation model, we derive a model for transient film boiling dynamics. We investigate the stability of its steady-state solution by locally applying potential flow linear stability analysis. We show how the behavior will be an inclination dependent mixture of Kelvin–Helmholtz and Rayleigh–Taylor type instabilities, and a relatively simple stability criterion is derived. We also show how the transient lubrication model is incapable of predicting the former kind of instability. The model's ability to predict the inclination dependence of stability limits is tested against an experimental data set from the literature, and we see that the model displays reasonable accuracy considering its lack of free empirical parameters.

Keywords: Film boiling, Liquid–vapor interface, Thin vapor film, Stability, Inclination angle, Kelvin–Helmholtz

1. Introduction

When a heated solid surface is submerged in a liquid with a considerably lower saturation temperature, a vapor phase will begin to nucleate at the surface of contact. The resulting relationship between the surface superheat and the heat flux is the *boiling curve* (Dhir, 1998), also called the Nukiyama curve, named after the person who first characterized it in the 1930s (Nukiyama, 1934). At moderate superheat, in the nucleate boiling regime, the boiling curve exhibits the intuitive behavior of increasing heat flux with increasing superheat. However, this will only continue up to the *critical heat flux* (CHF), which signals the transition from *nucleate boiling* to *film boiling*, and is seen as a counterintuitive decrease in heat flux with increasing surface temperature. The drop in heat flux is due to the formation of a continuous vapor film between the solid and the liquid, which has an insulating effect on the heat transfer. In some practical situations film boiling is desirable, and in some it is not. In either case it is of interest to predict the dynamics of the vapor film, and under which conditions it may become unstable. Instabilities indicate a change in heat transfer properties, and may also precede vapor film collapse (Leidenfrost point) (Dhir, 1998).

Predicting the overall heat transfer efficiency of film boiling is important for various industrial concerns. This includes the relatively common case of quenching hot solid surfaces with water (Dhir, 1998), but also the more exotic case of cryogens boiling when spreading on top of water (Hissong, 2007). The stability limits and breakdown of film boiling are also important, as they are believed to be the triggering mechanism for vapor explosions (rapid phase transition) in nuclear fuel-coolant interactions (Fletcher, 1995; Berthoud, 2000) and liquefied natural gas (LNG) (Luketa-Hanlin, 2006; Cleaver et al., 2007).

The problem to be solved in this work is illustrated in Fig. 1. This is a case of two-dimensional saturated natural convection film boiling on a heated solid plate. Since the model assumes a state of film boiling, it is only applicable at surface temperatures above the value at the fluid's CHF. At the same time, it is assumed that the surface temperature is low enough that radiation heat transfer may be neglected. As shown by Jouhara and Axcell (2009), this is valid for quite a wide range of surface temperatures.

The objective is to predict the spatiotemporal behavior of the liquid–vapor interface, mathematically represented by the film thickness function $h(x,t)$. The plate is submerged at a given angle α, and particular attention is given to how the dynamics change depending on this inclination. Under common conditions the formed vapor film is very thin, of the order of 100 µm (Dhir, 1998; Jouhara and Axcell, 2002). Since this is likely to be much thinner than the tangential length scale, thin-film flow theory is applicable for the analysis of the vapor film dynamics. A common way of approaching thin-film flow is by use of the *lubrication approximation* (Kundu et al., 2007, Sec. 8.3),

https://doi.org/10.1016/j.ijmultiphaseflow.2018.05.010
*Corresponding author
Email address: eskil.aursand@ntnu.no (Eskil Aursand)

which exploits the large difference in length scales in order to simplify the Navier–Stokes equations. When combined with the mass-conservation principle, this will reduce the full set of governing equations and boundary conditions to a single highly nonlinear scalar PDE (Myers, 1998).

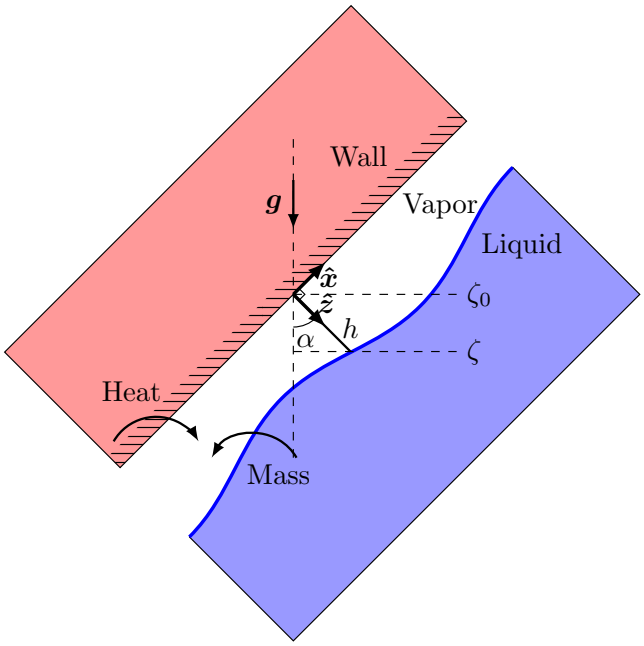

Figure 1: Illustration of the planar film boiling problem. A wall at angle α supplies heat to a boiling liquid, which feeds vapor into the vapor film in between. Buoyancy then drives vapor flow along the wall.

The dynamics of thin liquid films on solid surfaces, including analysis by the lubrication approximation, has been extensively reviewed in the past by Oron et al. (1997), Myers (1998) and Craster and Matar (2009). Considerable analysis has been done specifically on horizontal evaporating or condensing liquid films, e.g. by Burelbach et al. (1988). The case of an evaporating liquid film falling down an inclined plane has been treated by authors such as Joo et al. (1991). The case of film boiling is different, as the thin film consists of vapor, not liquid. Some work has been done on analyzing film boiling dynamics with thin-film models, such as in Panzarella et al. (2000), Kim et al. (2015) and Kim and Kim (2016). However, these were for the purely horizontal case, with no net tangential flow or significant shear forces. In terms of stability analysis, horizontal film boiling has uniform but time-dependent base states. The vertical and inclined cases are different, as they have steady but non-uniform base states. Such steady solutions have been studied since the work of Bromley (1950) in the 50s, and have since been elaborated by many authors, such as Koh (1962), Bui and Dhir (1985), Kolev (1998) and Jouhara and Axcell (2009). While they show some variations due to different assumptions regarding liquid dynamics outside the film, most have the same general form of $h \sim x^{1/4}$, with x being the distance along the solid surface. There are few works on film boiling considering the effect of inclination away from the vertical. Examples are Nishio and Chandratilleke (1991) and Kim and Suh (2013).

The purpose of the present study is to investigate the limits of stability of the steady solutions found in non-horizontal film boiling. Particular attention is given to the interplay of Kelvin–Helmholtz and Rayleigh–Taylor instability mechanisms, and how this depends on inclination angle. The goal is to achieve this analysis with a relatively simple model, in order to gain insight and practically useful expressions. While Kim and Suh (2013) consider the inclination dependence of film boiling stability, the actual onset of instability in their model is given by the *critical Reynolds number*, an empirical parameter that is fitted to the experiments. The present work avoids any free empirical parameters, and thus offers ab initio predictions on stability.

In Sec. 2 we derive a transient model for inclined planar saturated film boiling based on the lubrication approximation. The result is a fourth-order highly nonlinear parabolic PDE for the vapor film thickness. We show that the equation has an analytical approximate steady-state solution, with a corresponding expression for the average tangential vapor velocity.

In Sec. 3 we show how scales based on these steady solutions can give a useful dimensionless formulation of the model based on a few dimensionless numbers. We highlight how the values of these numbers depend on position and orientation. In Sec. 4 we find under which conditions the previously found steady-state solutions will turn unstable, and which wavelengths will be prominent once that occurs. This is done in two different ways. First, this is done by performing linear stability analysis of the PDE from the lubrication approximation, and then by locally applying potential flow stability analysis to the steady-state solution from the lubrication model. Both lead to their own stability criteria, with some similarities and some differences. As will be shown, the former method lacks predictive capabilities for a prominent stability mechanism. We go on to analyze why.

In Sec. 5 we leave the dimensionless world for a while in order to show practical results for a specific case involving water film boiling over a range of superheat degrees. In Sec. 6 we compare predictions from the stability analysis with certain experimental measurements by Kim and Suh (2013). Finally, the important messages of the present study are summed up in Sec. 7.

2. Lubrication approximation model

We aim to model the behavior of the film thickness function $h(x,t)$, in the setup illustrated in Fig. 1. In order to do this, we make the following assumptions:

- We assume that the thickness of the film is much smaller than its length scale. This allows the application of the lubrication approximation.
- We assume that the thermo-physical properties of the vapor, such as density and viscosity, can be treated as constant.
- We assume that the evaporation rate is small enough that it is in quasi-equilibrium, thus locking the interface temperature to the saturation temperature. This has the secondary effect of also neglecting any thermo-capillary effects, since the interface temperature will be constant.
- We neglect any effect the liquid dynamics may have on pressure, i.e. the interface pressure on the liquid side is given by the hydrostatic pressure.
- The pressure jump across the liquid–vapor interface is given by surface tension alone, i.e. we are neglecting the vapor thrust effect.
- We neglect any van der Waals contributions to the film pressure (disjoining pressure).

2.1. Mass flow rate from lubrication approximation

In the case of thin-film flow of an incompressible fluid, we may apply the classical lubrication approximation (Kundu et al., 2007, Sec. 8.3). This assumption uses the large difference in the film's tangential and perpendicular length scales to neglect the inertial and time-differential terms in the Navier–Stokes equations. The momentum equations reduce to

$$\frac{\partial p}{\partial x} = \rho_\mathrm{v} g_x + \mu_\mathrm{v} \frac{\partial^2 u}{\partial z^2}, \tag{1}$$

and

$$\frac{\partial p}{\partial z} = \rho_\mathrm{v} g_z. \tag{2}$$

Here p is the pressure, u is the x-directed velocity, μ_v is the vapor viscosity, ρ_v is the vapor density, and g_x, g_z are the gravitational acceleration projected along the x and z-directions, respectively. According to the definition of the inclination angle α in Fig. 1, we have that

$$g_x = -g \sin\alpha, \tag{3}$$
$$g_z = g \cos\alpha, \tag{4}$$

where g is the gravitational acceleration. Under the assumption that $\partial p/\partial x$ is independent of z, which will be justified in Sec. 2.2, we find from Eq. (1) that the second derivative of u with respect to z is constant at a given x, and can be written as

$$\frac{\partial^2 u}{\partial z^2} = -\frac{1}{\mu_\mathrm{v}} D(x), \tag{5}$$

where we have defined the driving force $D(x)$,

$$D(x) \equiv \rho_\mathrm{v} g_x - \frac{\partial p}{\partial x}. \tag{6}$$

The expression in Eq. (5) implies a parabolic velocity profile with a given curvature. In order to find this profile we need two additional pieces of information, and these are the boundary conditions at the solid wall ($z = 0$) and at the liquid-vapor interface ($z = h$). At the solid wall, the no-slip condition simply implies that $u = 0$. At the liquid–vapor interface, we assume continuity of tangential velocity and shear stress. Here we will make no specific assumptions about the interface tangential velocity, but rather investigate the two extreme possibilities: These are the assumption of zero velocity ($u = 0$), and the assumption of zero shear stress at the interface ($\partial u/\partial z = 0$). In either case, this leads to the same kind of expression for the mass flow rate along the film,

$$M(x) = W \frac{\rho_\mathrm{v} h^3}{\beta \mu_\mathrm{v}} D(x), \tag{7}$$

where W is the depth of the film in the symmetry direction, and the difference from the two assumptions enter through the factor β, with values

$$\beta = \begin{cases} 12 & \text{Maximum shear stress.} \\ 3 & \text{Zero shear stress.} \end{cases} \tag{8}$$

When $\beta = 12$, the tangential interface velocity is zero. When $\beta = 3$, the tangential interface velocity is 3/2 times the average vapor velocity. In reality, the value of β would be somewhere in between, but we see that in any case the order of magnitude of $M(x)$ stays the same. A discussion on estimating the actual value of β from the viscosity ratio can be found in Appendix A.

2.2. Pressure model

In order to use the expression Eq. (7), we will need a model for the driving force Eq. (6), and thus the pressure gradient $\partial p/\partial x$ in the film. With the boundary condition $p(z = h) = p_\mathrm{v,i}$, the solution to Eq. (2) is

$$p = p_\mathrm{v,i} - \rho_\mathrm{v} g_z \left(h - z\right), \tag{9}$$

where $p_\mathrm{v,i}$ is the pressure at the vapor side of the liquid-vapor interface. Since neither $p_\mathrm{v,i}$ nor h are functions of z, we see that $\partial p/\partial x$ will be independent of z, as assumed earlier. The pressure jump at the interface is given by the surface tension contribution,

$$p_\mathrm{l,i} - p_\mathrm{v,i} = \sigma\kappa, \tag{10}$$

where $p_\mathrm{l,i}$ is the interface pressure on the liquid side, σ is the surface tension, and κ is the interface curvature. The curvature can be calculated from the film thickness function by

$$\kappa = \frac{\frac{\partial^2 h}{\partial x^2}}{\left(1 + \left(\frac{\partial h}{\partial x}\right)^2\right)^{3/2}} \approx \frac{\partial^2 h}{\partial x^2}, \tag{11}$$

where the final approximation can be used for long waves where $\partial h/\partial x \ll 1$, which will be applicable here. The liquid pressure at the interface is given by the hydrostatic contribution corresponding to the vertical position of the interface,

$$p_{\mathrm{l,i}} = p_0 - \rho_{\mathrm{l}} g \zeta, \tag{12}$$

where p_0 is a reference pressure, ρ_{l} is the liquid density, and $\zeta = \zeta_0 - h\cos(\alpha)$ is the vertical position of the interface (see Fig. 1). The latter depends on x as

$$\frac{\partial \zeta}{\partial x} = \sin(\alpha) - \cos(\alpha)\frac{\partial h}{\partial x}. \tag{13}$$

If we combine Eqs. (9), (10), (12) and (13), we find that

$$\frac{\partial p}{\partial x} = -\rho_{\mathrm{l}} g \sin(\alpha) + \Delta\rho g \cos(\alpha)\frac{\partial h}{\partial x} - \sigma\frac{\partial \kappa}{\partial x}, \tag{14}$$

where $\Delta\rho \equiv \rho_{\mathrm{l}} - \rho_{\mathrm{v}}$. The driving force is thus given by

$$D(x) = \Delta\rho g\left[a + b\frac{\partial h}{\partial x}\right] + \sigma\frac{\partial \kappa}{\partial x}, \tag{15}$$

where we have defined the short-hands

$$a = \sin\alpha, \tag{16}$$

$$b = -\cos\alpha. \tag{17}$$

Note that in this pressure model both the vapor thrust and van der Waals terms have been neglected, for the same reasons as those presented by Panzarella et al. (2000).

2.3. Heat transfer and evaporation

The evaporation is driven by a heat flux across the vapor film, caused by a temperature difference between the wall and the liquid-vapor interface. When considerable evaporation or condensation occurs across a liquid–vapor interface, the liquid interface temperature T_{i} is not actually exactly at the thermodynamic saturation temperature T_{sat} of the fluid. For moderate evaporation rates, we may linearize this effect through the following constitutive equation,

$$T_{\mathrm{i}} - T_{\mathrm{sat}} = Kj, \tag{18}$$

where j is the evaporation mass flux, and K is the non-equilibrium coefficient whose value can be estimated from kinetic gas theory (Burelbach et al., 1988; Oron et al., 1997; Panzarella et al., 2000). For strong evaporation there may also be a slight temperature discontinuity at the liquid-vapor interface. In this work we take the quasi-equilibrium limit, which implies a temperature that is continuous, and equal to the saturation temperature at the interface, i.e. $T_{\mathrm{i}} = T_{\mathrm{sat}}$. In fact, we state that the entire bulk of the liquid is at the temperature T_{sat}, i.e. we have so-called *saturated film boiling*. This has the consequence that all the heat conducted into the interface from the vapor side is spent on evaporation. Accounting for any further heating of the liquid above T_{sat} would require a non-equilibrium model.

With the lubrication approximation, the energy equation in the vapor film reduces to

$$\frac{\partial^2 T}{\partial z^2} = 0, \tag{19}$$

i.e. the temperature profile is linear. This means that in this approximation, the heat flux conducted into the liquid–vapor interface is equal to the heat flux conducted from the wall to the vapor. In reality, some energy must be spent heating the newly added vapor from T_{sat} to the temperature in the vapor film, the so-called *sensible heat* effect, but this is negligible when the lubrication approximation applies. If one wanted to account for this, it may be achieved by slightly adjusting the effective latent heat of evaporation, and therefore it will not affect the qualitative conclusions of this work.

Since the liquid is assumed to be uniformly at its saturated state, all heat reaching the liquid–vapor interface will be spent on evaporation. This energy balance can be expressed as

$$\dot{q}|_{z=h} = Lj \tag{20}$$

where $\dot{q}$ is the heat flux and L is the latent heat of evaporation. Since we stay in the regime of negligible radiation heat, the heat flux reaching the liquid–vapor interface is given by Fourier's law alone, which states that

$$\dot{q}|_{z=h} = k_{\mathrm{v}}\left.\frac{\partial T}{\partial z}\right|_{z=h} = k_{\mathrm{v}}\frac{\Delta T}{h}, \tag{21}$$

where the last equality follows from Eq. (19). Here, k_{v} is the vapor thermal conductivity and ΔT is the difference between wall temperature and saturation temperature (wall superheat). If we combine Eq. (20) and Eq. (21), we may write the mass flux as a function of film thickness,

$$j = \frac{Q}{h}, \tag{22}$$

where we have defined the constant

$$Q = \frac{k_{\mathrm{v}}\Delta T}{L}. \tag{23}$$

2.4. Mass conservation

We now consider mass conservation in a control volume of vapor film from x_{L} to x_{R}, i.e. of length $\Delta x = x_{\mathrm{R}} - x_{\mathrm{L}}$. The conservation principle implies that the rate of change of mass contained in this volume of vapor film must be equal to the net mass flow rate into it. With a constant density, this becomes

$$\begin{aligned} &W\rho_{\mathrm{v}}\frac{\partial}{\partial t}\int_{x_{\mathrm{L}}}^{x_{\mathrm{R}}} h(x)\mathrm{d}x + M(x_{\mathrm{R}}) - M(x_{\mathrm{L}}) \\ &= W\int_{x_{\mathrm{L}}}^{x_{\mathrm{R}}} j(x)\mathrm{d}x \end{aligned} \tag{24}$$

Given the mass flow rate of Eq. (7) and an evaporation mass flux model of the form Eq. (22), Eq. (24) becomes

$$\frac{\partial}{\partial t}\int_{x_\mathrm{L}}^{x_\mathrm{R}} h(x)\mathrm{d}x + \frac{h^3(x_\mathrm{R})}{\beta\mu_\mathrm{v}}D(x_\mathrm{R}) - \frac{h^3(x_\mathrm{L})}{\beta\mu_\mathrm{v}}D(x_\mathrm{L}) = \frac{Q}{\rho_\mathrm{v}}\int_{x_\mathrm{L}}^{x_\mathrm{R}} \frac{1}{h(x)}\mathrm{d}x \tag{25}$$

In the limits $\Delta x \to 0$ and $h \gg \Delta x$, Eq. (25) reduces to the PDE

$$\frac{\partial h}{\partial t} + \frac{1}{\beta\mu_\mathrm{v}}\frac{\partial}{\partial x}\left[h^3\left(\Delta\rho g\left(a + b\frac{\partial h}{\partial x}\right) + \sigma\frac{\partial \kappa}{\partial x}\right)\right] = \frac{Q}{\rho_\mathrm{v} h}, \tag{26}$$

which is the governing equation for the film thickness $h(x,t)$ in this set of approximations.

2.5. Approximate steady-state solution

We seek a steady-state solution to this problem, $\bar{h}(x)$, and assume that such a solution will be so slowly varying in space that the surface tension contribution to the mass flow rate is negligible. The full equation Eq. (25) then reduces to

$$\left(\bar{h}^3\left[a + b\frac{\partial \bar{h}}{\partial x}\right]\right)_\mathrm{R} - \left(\bar{h}^3\left[a + b\frac{\partial \bar{h}}{\partial x}\right]\right)_\mathrm{L} = \frac{\beta\mu_\mathrm{v} Q}{\rho_\mathrm{v}\Delta\rho g}\int_{x_\mathrm{L}}^{x_\mathrm{R}} \frac{1}{\bar{h}(x)}\mathrm{d}x. \tag{27}$$

It turns out that an exact analytical solution to Eq. (27) can be found, and it is

$$\bar{h}(x) = \left(\frac{4\beta}{3}\frac{\mu_\mathrm{v} Q}{\rho_\mathrm{v}\Delta\rho g a}\right)^{1/4} x^{1/4}. \tag{28}$$

Curiously, the solution Eq. (28) is independent of b. This is possible because solutions in the form $\bar{h} \sim x^{1/4}$ has the property that $\bar{h}^3\partial\bar{h}/\partial x$ is constant, and thus the contribution of the b-term to the flux gradient is zero.

A steady-state solution with the properties $\bar{h} \sim x^{1/4}$ and $\bar{h} \sim a^{-1/4}$ has been presented before by authors such as Nishio and Chandratilleke (1991) and Kim and Suh (2013). However, Eq. (28) includes the factor β, which in a simple way shows the effects of the possible range of assumptions that could be made for the liquid flow. What is typically not discussed in relation to this solution is its inconsistency with the lubrication approximation in the $h(x) \to 0$ limit. Physically, we would expect the mass flow rate $M(x)$ to approach zero, but with the expression in Eq. (15), $h^3 D(x)$ and thus $M(x)$ incorrectly approaches a finite value, giving infinite velocity. Fortunately this error is small for small aspect ratios and/or inclinations close to vertical.

If we accept the film thickness function given by Eq. (28), we may calculate the average vapor velocity at position x by considering total mass conservation,

$$\begin{aligned}\bar{u}(x) &= \frac{Q}{\rho_\mathrm{v}\bar{h}(x)}\int_0^x \frac{1}{\bar{h}(x')}\mathrm{d}x' \\ &= \frac{\Delta\rho g a}{\beta\mu_\mathrm{v}}\bar{h}^2(x) \\ &= \sqrt{\frac{4}{3\beta}\frac{\Delta\rho g Q a}{\mu_\mathrm{v}\rho_\mathrm{v}}}\sqrt{x}.\end{aligned} \tag{29}$$

The above shows the dependence of $\bar{u}$ on both position x and the position-dependent film thickness $\bar{h}$. Both are useful forms. The vapor velocity will increase in proportion to $\sqrt{x}$, and as we will see, eventually the velocities will be large enough for Kelvin–Helmholtz instabilities to be important.

3. Scales and dimensionless numbers

3.1. Scales of film boiling dynamics

A planar film boiling case is given by fluid properties, an inclination angle α, a superheat ΔT, and a plate length x_0. We define the scales of a given case by the steady-state solution Eq. (28) at $x = x_0$. In order to highlight the effects of inclination, we use the corresponding vertical ($a = 1$) case as a reference. Thus the length scale, used for both x and z, is

$$h_0 = \left(\frac{4\beta}{3}\frac{\mu_\mathrm{v} Q}{\rho_\mathrm{v}\Delta\rho g}x_0\right)^{1/4} = a^{1/4}\bar{h}(x_0). \tag{30}$$

We use the average vapor velocity as the velocity scale,

$$u_0 = \frac{\Delta\rho g}{\beta\mu_\mathrm{v}}h_0^2 = \sqrt{\frac{4}{3\beta}\frac{\Delta\rho g Q}{\mu_\mathrm{v}\rho_\mathrm{v}}x_0} = \frac{\bar{u}(x_0)}{\sqrt{a}}. \tag{31}$$

This enables us to define a time scale,

$$t_0 = \frac{h_0}{u_0} = \frac{\beta\mu_\mathrm{v}}{\Delta\rho g h_0} = \left(\frac{3\beta^3\mu_\mathrm{v}^3\rho_\mathrm{v}}{4Qx_0(\Delta\rho g)^3}\right)^{1/4}. \tag{32}$$

3.2. Dimensionless numbers

The dimensionless numbers used in this work, and their common definitions, are shown in Tab. 1. If we insert the film thickness Eq. (28) and the velocity Eq. (29) into the general definitions in Tab. 1, we get the film-boiling specific expressions,

$$\mathrm{Bo} = \frac{\Delta\rho g h^2}{\sigma} = \frac{1}{\sigma}\sqrt{\frac{4\beta\Delta\rho g\mu_\mathrm{v} Q}{3\rho_\mathrm{v} a}x_0}, \tag{33}$$

$$\mathrm{Re} = \frac{\rho_\mathrm{v}\Delta\rho g a h^3}{\beta\mu_\mathrm{v}^2} = \left(\frac{64\rho_\mathrm{v}\Delta\rho g Q^3 a}{27\beta\mu_\mathrm{v}^5}x_0^3\right)^{1/4}, \tag{34}$$

Table 1: Summary of dimensionless numbers used in this work, and their common definitions.

Name	Definition	Description
Bond number	$\mathrm{Bo} = \frac{\Delta\rho g h^2}{\sigma}$	Buoyant vs capillary forces.
Reynolds number	$\mathrm{Re} = \frac{\rho_\mathrm{v} u h}{\mu_\mathrm{v}}$	Inertial vs viscous forces.
Weber number	$\mathrm{We} = \frac{\rho_\mathrm{v} u^2 h}{\sigma}$	Inertial vs capillary forces.
Aspect ratio	$\epsilon = \frac{h}{x_0}$	Film thickness vs film length.

$$\mathrm{We} = \frac{\rho_\mathrm{v}(\Delta\rho g)^2 a^2 h^5}{\beta^2 \sigma \mu_\mathrm{v}^2} = \frac{1}{\sigma}\left(\frac{1024(\Delta\rho g)^3 Q^5 a^3 x_0^5}{243\beta^3 \rho_\mathrm{v}\mu_\mathrm{v}^3}\right)^{1/4}, \tag{35}$$

$$\epsilon = \frac{h}{x_0} = \left(\frac{4\beta\mu_\mathrm{v} Q}{3\rho_\mathrm{v}\Delta\rho g a x_0^3}\right)^{1/4}. \tag{36}$$

We see that in the film boiling case, we have the relation

$$\mathrm{We} = \frac{a\mathrm{ReBo}}{\beta}, \tag{37}$$

since the buoyant and viscous forces become directly related in the lubrication approximation. When referring to the reference (vertical) case, we add a subscript 0 to the dimensionless numbers. The angular dependence of these numbers are

$$\mathrm{Bo} = a^{-1/2}\mathrm{Bo}_0, \tag{38}$$
$$\mathrm{Re} = a^{1/4}\mathrm{Re}_0, \tag{39}$$
$$\mathrm{We} = a^{3/4}\mathrm{We}_0, \tag{40}$$
$$\epsilon = a^{-1/4}\epsilon_0. \tag{41}$$

In some cases it is useful to substitute the full plate length x_0 for the film thickness h in the definition of the Bond number. We label this Bo_X, and it is defined as

$$\mathrm{Bo}_X = \frac{\Delta\rho g x_0^2}{\sigma}. \tag{42}$$

An overview of typical values for these scales and dimensionless numbers is shown in Tab. 2.

Table 2: Overview of possible values for scales and dimensionless numbers, here for boiling water with case parameters ΔT = 100–200 K and X_0 = 0.5–10 cm. These ranges of ΔT and X_0 yield a range of values for each scale and dimensionless number, based on expressions found in Sec. 3. The max/min limits of these ranges are shown in this table.

	Min	Max	Unit	Eq.
h_0	120	300	µm	(30)
u_0	0.94	6.0	$\mathrm{m\,s^{-1}}$	(31)
t_0	0.048	0.12	ms	(32)
Bo_0	0.0021	0.013	–	(33)
Re_0	5.3	84	–	(34)
We_0	0.0010	0.10	–	(35)
ϵ_0	0.0024	0.027	–	(36)
Bo_X	4.0	1600	–	(42)

4. Linear stability analysis

We now wish to investigate the conditions where the steady-state solution Eq. (28) is stable with respect to small perturbations. This is done by two different approaches:

- In Sec. 4.1, we apply linear stability analysis to the dimensionless version of the PDE from the lubrication approximation, Eq. (26).
- In Sec. 4.2, we use the classical result from potential flow stability analysis for the shear flow of two immiscible fluids in a gravitational field. We then use the steady-state solution from the lubrication approximation to insert expressions for the vapor film thickness and the velocities on either side of the interface.

As will be shown, the two approaches give consistent results in some respects, but will also have significant qualitative differences.

4.1. Lubrication approximation

4.1.1. Dispersion relation

If we use the length and time scales defined in Sec. 3.1, as well as the approximate expression for curvature in Eq. (11), the PDE in Eq. (26) can be written in dimensionless form as

$$\frac{\partial H}{\partial \tau} + \frac{\partial}{\partial X}\left[H^3\left(a + b\frac{\partial H}{\partial X} + c\frac{\partial^3 H}{\partial X^3}\right)\right] = \frac{3\epsilon_0}{4}\frac{1}{H}, \tag{43}$$

where H, τ and X are the dimensionless film thickness, time and position, respectively, and we have defined $c = 1/\mathrm{Bo}_0$. Eq. (43) can be classified as a fourth-order nonlinear parabolic equation with a source term. Such thin-film equations with inclination have been studied previously by e.g. Myers (1998), but commonly in the context of falling liquid films, not buoyant vapor films. The specific form in Eq. (43) may be solved numerically by semi-implicit methods, as demonstrated by Aursand (2017).

The steady-state solution Eq. (28) takes on an especially simple dimensionless form,

$$\bar{H}(X) = \left(\frac{\epsilon_0 X}{a}\right)^{1/4}. \tag{44}$$

This is thus a steady-state solution of Eq. (43) for $c = 0$. We see that for a vertical plate, $\bar{H}(1/\epsilon_0) = 1$, as was intended by the scaling. We now investigate the stability of a steady solution $\bar{H}(X)$ by considering solutions to Eq. (43) that are equal to the steady solution with a small added transient perturbation, $H(X,\tau) = \bar{H}(X) + \eta(X,\tau)$. The perturbation can be written as $\eta(x,t) = Af(X,\tau)$, where A is a small number giving the magnitude of the perturbation, and $f(X,\tau)$ is the shape of the perturbation. If we insert this into Eq. (43), use Eq. (44) for $\bar{H}(x)$ and its derivatives, and assume that $\bar{H}(x) \sim \mathcal{O}(1)$, we obtain the following PDE for the perturbation $\eta(X,\tau)$,

$$\begin{aligned}&\frac{\partial \eta}{\partial \tau} + c\bar{H}^3\frac{\partial^4 \eta}{\partial X^4} + \frac{3c\epsilon_0}{4\bar{H}a}\frac{\partial^3 \eta}{\partial X^3} + b\bar{H}^3\frac{\partial^2 \eta}{\partial X^2}\\ &+ \left(3a\bar{H}^2 + \frac{3b\epsilon_0}{2\bar{H}a}\right)\frac{\partial \eta}{\partial X} + \frac{9\epsilon_0}{4\bar{H}^2}\eta\\ &= \mathcal{O}\left(A^2\right) + \mathcal{O}\left(\epsilon_0^2\right),\end{aligned} \tag{45}$$

We may then investigate the initial evolution of a plane wave disturbance $f(x,t) = \exp\left[i\left(kX - \omega\tau\right)\right]$, where k is the wavenumber and ω is the complex angular frequency. If we insert this form for η into the PDE Eq. (45), and discard the higher order terms in A and ϵ_0, we get the following dispersion relation,

$$\begin{aligned}\omega =& 3a\bar{H}^2 k + \frac{3b\epsilon_0}{2\bar{H}a}k - \frac{3c\epsilon_0}{4\bar{H}a}k^3\\ &+ i\left[\bar{H}^3 k^2\left(b - ck^2\right) - \frac{9\epsilon_0}{4\bar{H}^2}\right].\end{aligned} \tag{46}$$

4.1.2. Stability

The disturbance is unstable if the imaginary part of ω is positive. We see that in this model, the only source of instability is the b-term (Rayleigh-Taylor type buoyant effect), and this will be present only if $b > 0$. When $b > 0$, we have unconditional stabilization due to surface tension for all wavenumbers above the maximum value $k_{\max}^2 = b\mathrm{Bo}_0$. Additionally, there is the evaporation term (ϵ_0-term) which stabilizes all wavenumbers equally. However, its effect is most noticeable for small k, where surface tension has little effect. Thus, for positive b there is a potential for instabilities, but surface tension stabilizes short wavelengths, and evaporation stabilizes long wavelengths.

We see from Eq. (46) that the largest potential for instability is where $\bar{H}$ is largest, i.e. where $\bar{H} = a^{-1/4}$. In order to investigate total stability, we look at the stability at this point. For $b > 0$, there is instability between the critical wavenumbers,

$$k_{\mathrm{crit}}^2 = \frac{1}{2c}\left(b \pm \sqrt{b^2 - 9c\epsilon_0 a^{5/4}}\right). \tag{47}$$

However, for a given case with plate length x_0, not all wavenumbers are available for excitation. If we decide that wavelengths larger than x_0 are not allowed, we get a minimum allowable dimensionless wavenumber of $k_{\min} = 2\pi\epsilon_0$. A sufficient and necessary criterion for stability is that $k_{\min} > k_{\mathrm{crit}}$, which can be stated as

$$4\pi^2 > b\mathrm{Bo}_X\frac{1}{2}\left(1 + \sqrt{1 - \frac{9a^{5/4}}{\epsilon_0\mathrm{Bo}_X b^2}}\right). \tag{48}$$

The above criterion is quite unwieldy, but we may also state simpler sufficient (but not necessary) criteria for stability. These are

$$b\mathrm{Bo}_X < 4\pi^2, \tag{49}$$

$$\frac{b^2}{a^{5/4}} < \frac{9}{\epsilon_0\mathrm{Bo}_X}. \tag{50}$$

Either one of these is sufficient for stability. Eq. (49) is satisfied when all allowable wavelengths are stabilized by surface tension. Eq. (50) is satisfied when the evaporation effect is sufficient to stabilize all wavelengths until the end of the plate. Note that Eq. (48) is satisfied for all $b \leq 0$ regardless of other conditions, and thus the vertical case and all liquid-below-vapor orientations are predicted to be stable.

The most dangerous (fastest growing) wavenumber can be found as the value of k giving the largest imaginary value in Eq. (46),

$$k_{\mathrm{d}}^2 = \frac{1}{2}b\mathrm{Bo}_0, \tag{51}$$

which in the horizontal ($b = 1$) limit agrees with the common Rayleigh–Taylor instability result from lubrication theory (Kim et al., 2015).

4.2. Potential flow

4.2.1. General thin-film flow

We now disregard evaporation for a moment, and consider the case of a thin vapor film of constant thickness h, with a solid wall on one side, and an infinite liquid on the other side. The vapor and the liquid both have a given base state velocity, u_{v} and u_{l}, respectively. If we apply potential flow linear stability analysis (Drazin and Reid, 2004) to the liquid–vapor interface in this model case, the dispersion relation for a small harmonic disturbance ($\sim \exp\left(i[\tilde{k}x - \tilde{\omega}t]\right)$) becomes

$$\begin{aligned}\tilde{\omega} =& \frac{\tilde{k}\left(\rho_{\mathrm{l}}u_{\mathrm{l}} + \rho'_{\mathrm{v}}u_{\mathrm{v}}\right)}{\rho_{\mathrm{l}} + \rho'_{\mathrm{v}}}\\ &\pm\left(\frac{\tilde{k}^3\sigma}{\left(\rho_{\mathrm{l}} + \rho'_{\mathrm{v}}\right)} + \frac{\tilde{k}g_z\Delta\rho}{\left(\rho_{\mathrm{l}} + \rho'_{\mathrm{v}}\right)} - \frac{\tilde{k}^2\rho_{\mathrm{l}}\rho'_{\mathrm{v}}(u_{\mathrm{v}} - u_{\mathrm{l}})^2}{(\rho_{\mathrm{l}} + \rho'_{\mathrm{v}})^2}\right)^{\frac{1}{2}}.\end{aligned} \tag{52}$$

where $\tilde{\omega}$ is the dimensional complex angular frequency, $\tilde{k}$ is the dimensional wavenumber, and we have introduced

the following shorthand for the effective vapor density due to the thin-film effect,

$$\rho_{\mathrm{v}}' = \frac{\rho_{\mathrm{v}}}{\tanh(\tilde{k}h)}. \tag{53}$$

We may state Eq. (52) in dimensionless form by choosing a length scale h_0 and a velocity scale u_0. The result is in the form

$$\omega = \omega_{\mathrm{R}} \pm \omega_{\mathrm{I}}, \tag{54}$$

where ω_{R} is always real, while ω_{I} is imaginary in the case of instabilities. The latter turns out to be

$$\omega_{\mathrm{I}} = \left(\frac{\sigma}{h_0 u_0^2 \rho_{\mathrm{l}} \left(1 + \frac{\rho_{\mathrm{v}}'}{\rho_{\mathrm{l}}}\right)}\right)^{\frac{1}{2}} \left(k^3 - b\mathrm{Bo}_0 k - \left(\frac{u_{\mathrm{v}}}{u_0}\right)^2 \left(1 - \frac{u_{\mathrm{l}}}{u_{\mathrm{v}}}\right)^2 \frac{\rho_{\mathrm{v}}'}{\rho_{\mathrm{v}}} \frac{\mathrm{We}_0 k^2}{1 + \frac{\rho_{\mathrm{v}}'}{\rho_{\mathrm{l}}}}\right)^{\frac{1}{2}}, \tag{55}$$

Here ω and k are the dimensionless angular frequency and wavenumber, respectively, according to the length scale h_0 and the time scale h_0/u_0. We have introduced Bo_0 and We_0 according to their definitions in Tab. 1 using h_0 and u_0. We allow the actual film thickness to be different from the scale h_0, and the deviation is given by the dimensionless film thickness H, such that $\tilde{k}h = kH$. Under the assumption that the waves are long but not extremely long,

$$\frac{\rho_{\mathrm{v}}}{\rho_{\mathrm{l}}} \ll kH \ll 1, \tag{56}$$

an assumption that will be checked for self consistency later, we may perform the simplifications $\tanh(kH) \approx kH$ and $1 + \rho_{\mathrm{v}}'/\rho_{\mathrm{l}} \approx 1$ and thus simplify Eq. (55) to

$$\omega_{\mathrm{I}} = \left(\frac{\sigma}{h_0 u_0^2 \rho_{\mathrm{l}}}\right)^{\frac{1}{2}} \left(k^3 - b\mathrm{Bo}_0 k - \left(\frac{u_{\mathrm{v}}}{u_0}\right)^2 \left(1 - \frac{u_{\mathrm{l}}}{u_{\mathrm{v}}}\right)^2 \frac{\mathrm{We}_0 k}{H}\right)^{\frac{1}{2}}. \tag{57}$$

4.2.2. With steady-state film boiling solution

The result in Eq. (57) has so far not included anything specific to film boiling, but is simply an expression which, besides thermo-physical properties, requires three inputs in order to consider stability: A film thickness H, a characteristic vapor velocity u_{v}, and a characteristic liquid velocity u_{l}. We will now use the results from the steady-state lubrication analysis of film boiling to get values for these quantities. First, the dimensionless film thickness is given by Eq. (44), $\bar{H}(X) = (\epsilon_0 X/a)^{1/4}$. Second, we set the characteristic vapor velocity to be the average velocity in the film, $u_{\mathrm{v}} = \bar{u}$, according to Eq. (29). We can then see from Eq. (29) and Eq. (31) that at position X the ratio between average velocity and the velocity scale is

$$\frac{u_{\mathrm{v}}(X)}{u_0} = \sqrt{a\epsilon_0 X}. \tag{58}$$

Third, if we assume the characteristic liquid velocity to be about half of the interface velocity, we can use the result in Eq. (A.7) from Appendix A to state that

$$\frac{u_{\mathrm{l}}}{u_{\mathrm{v}}} = 1 - \frac{\beta}{12}. \tag{59}$$

If we insert all this into Eq. (57), we get

$$\omega_{\mathrm{I}} = \left(\frac{\sigma}{h_0 u_0^2 \rho_{\mathrm{l}}}\right)^{\frac{1}{2}} \left(k^3 - b\mathrm{Bo}_0 k - (\epsilon_0 X)^{\frac{3}{4}} a^{\frac{5}{4}} \left(\frac{\beta}{12}\right)^2 \mathrm{We}_0 k\right)^{\frac{1}{2}}. \tag{60}$$

Since Eq. (54) involves $\pm\omega_{\mathrm{I}}$, an imaginary ω_{I} will always enable an exponentially growing disturbance (instability). It will be imaginary if the contents of the last square root in Eq. (60) is negative. We see that there are two terms that contribute towards instability: A term with the Bond number Bo_0 which represents the Rayleigh–Taylor (RT) instability, and a term with the Weber number We_0 which represents the Kelvin–Helmholtz (KH) instability. We see that the RT term is equal at all positions, while the KH term increases as $X^{3/4}$ since the vapor velocity is larger further out in the film. Thus we have the highest potential for instability close to the end of the plate.

4.2.3. Limits of stability

We may now look at the conditions required for the film boiling to stay stable across a plate of a given physical length x_0. If the contents of the final square root in Eq. (60) is positive, we have stability. As mentioned, the highest potential for instability is at the end of the plate, where $\epsilon_0 X = 1$, so we will look for the conditions where this position will be stable. We can immediately see that the film will be stable with respect to very high k. Thus there may exist some critical wavenumber k_{crit} below which there may be instabilities. We find this as

$$k_{\mathrm{crit}}^2 = \mathrm{Bo}_0 \left(b + a^{5/4} \Phi_{\mathrm{KH}}\right), \tag{61}$$

where we have used the vertical special case of Eq. (37), $\mathrm{We}_0 = \mathrm{Re}_0 \mathrm{Bo}_0/\beta$, and defined the quantity

$$\Phi_{\mathrm{KH}} = \frac{\beta \mathrm{Re}_0}{144} \tag{62}$$

as the angle-independent relative importance of the KH instability. Given the typical ranges for Re_0 in Tab. 2, and given that $\beta \approx 10$, we see that $\Phi_{\mathrm{KH}} \in (0.35, 5.625)$. Since $\Phi_{\mathrm{KH}} \sim \mathcal{O}(1)$, we see that the KH instability will dominate close to the vertical configuration, and that the

RT instability will dominate close to the horizontal configuration.

While all wavenumbers $k < k_{\mathrm{crit}}$ can go unstable, not all the corresponding wavelengths can fit on the plate. If we again state that we only allow wavelengths shorter than the plate itself, we get a minimum allowable wavenumber of $k_{\mathrm{min}} = 2\pi\epsilon_0$. If $k_{\mathrm{min}} > k_{\mathrm{crit}}$ we can expect total stability, which leads to the stability condition

$$\frac{\mathrm{Bo}_X}{4\pi^2}\left(b + a^{5/4}\Phi_{\mathrm{KH}}\right) < 1. \tag{63}$$

In Eq. (63), all dependence on surface tension is contained in Bo_X. However, if the contents of the parenthesis is negative, we will have stability regardless of how weak the surface tension is. This may occur in the $\alpha < \pi/2$ region, if the KH instability is sufficiently balanced by a stabilizing RT effect. The limiting angle of this region, α_{min}, is given by

$$\frac{\cos(\alpha_{\mathrm{min}})}{\sin^{5/4}(\alpha_{\mathrm{min}})} = \Phi_{\mathrm{KH}}. \tag{64}$$

A decent approximation is then $\alpha_{\mathrm{min}} \approx \arctan(\Phi_{\mathrm{KH}}^{-1})$. Due to surface tension, the actual onset of instabilities will happen at some critical angle larger than α_{min}, where Eq. (63) is no longer satisfied. However the left hand side of Eq. (63) is not always monotonous with respect to angle α. If $\mathrm{Bo}_X < 4\pi^2$, i.e. if the plate length is of the order of the capillary length (or shorter), there is a potential for a return to stability as the angle starts to approach $\alpha \to \pi$. However, for any reasonable set of parameters this can only happen very close to $\alpha = \pi$, where the usage of the steady-state lubrication solutions becomes dubious anyway, so we will limit ourselves to looking for the first critical angle, α_{crit}, the smallest angle where Eq. (63) is satisfied as an equality.

In Fig. 2, we have numerically solved for α_{crit} in $(\mathrm{Bo}_X, \mathrm{Re}_0)$ space, while indicating typical parameter combinations occurring in the case of water film boiling. We see that at a given value of Bo_X, increasing Re_0 (e.g. by increasing ΔT) will cause instabilities to arise at smaller angles. It appears quite common that the critical angle will be far into the liquid-below-vapor region (blue regions in Fig. 2). In fact, for larger plate lengths instabilities can appear at $\alpha < 45°$ and lower, due to the high vapor velocities obtained. In the blue regions, the RT mechanism is stabilizing, so these instabilities are purely due to the KH mechanism.

4.2.4. Characteristic wavelengths

If we start out with a stable case, and slowly change a parameter to increase k_{crit} towards k_{min}, the instability that appears first will then obviously be $k \approx k_{\mathrm{min}}$, i.e. with the largest allowable wavelength. As we go further into the unstable region, the fastest growing allowable wavelength will keep being $k \approx k_{\mathrm{min}}$, until reaching the most dangerous wavenumber, k_{d}. Once k_{d} is within the range of allowed wavenumbers, it will be the dominant instability. See Fig. 3 for an illustration.

As before, the expression for k_{d} can be found as the value of k that gives the largest magnitude to ω_{I}, now found from Eq. (60). This turns out to be

$$k_{\mathrm{d}}^2 = \frac{1}{3}\mathrm{Bo}_0\left(b + a^{5/4}\Phi_{\mathrm{KH}}\right) = \frac{1}{3}k_{\mathrm{crit}}^2, \tag{65}$$

i.e the most dangerous wavelength is about 1.7 times the critical wavelength. We may show that the squared most dangerous wavelength ($\lambda_{\mathrm{d}} = 2\pi/k_{\mathrm{d}}$) becomes akin to a weighted harmonic (non-normalized) mean based on two other squared wavelengths, so that

$$\lambda_{\mathrm{d}}^2 = \left(b\frac{1}{\lambda_{\mathrm{RT}}^2} + a^{5/4}\frac{1}{\lambda_{\mathrm{KH}}^2}\right)^{-1}, \tag{66}$$

where λ_{RT} is the dimensionless Rayleigh–Taylor wavelength approached at the liquid-above-vapor horizontal configuration,

$$\lambda_{\mathrm{RT}} = 2\pi\sqrt{\frac{3}{\mathrm{Bo}_0}}, \quad \tilde{\lambda}_{\mathrm{RT}} = 2\pi\sqrt{\frac{3\sigma}{\Delta\rho g}}, \tag{67}$$

and λ_{KH} is the dimensionless Kelvin–Helmholtz wavelength approached at the vertical configuration,

$$\lambda_{\mathrm{KH}} = 2\pi\sqrt{\frac{3}{\frac{\beta^2}{144}\mathrm{We}_0}}, \quad \tilde{\lambda}_{\mathrm{KH}} = 2\pi\sqrt{\frac{3h_0\sigma}{\rho_{\mathrm{v}}\left(\frac{\beta}{12}u_0\right)^2}}, \tag{68}$$

with inclination-dependent weights $b = -\cos(\alpha)$ and $a^{5/4} = \sin^{5/4}(\alpha)$. The symbols $\tilde{\lambda}$ in Eqs. (67) and (68) indicate the corresponding dimensional wavelengths. These are consistent with the classical results from potential flow stability analysis. The ratio between the two wavelengths is

$$\frac{\lambda_{\mathrm{RT}}}{\lambda_{\mathrm{KH}}} = \sqrt{\Phi_{\mathrm{KH}}}. \tag{69}$$

Since $\Phi_{\mathrm{KH}} \sim \mathcal{O}(1)$, the wavelengths will mostly be of the same order of magnitude. Either could be somewhat larger than the other, and the point of equality is around $\mathrm{Re}_0 \approx 14$. Since Eq. (66) has the form of a harmonic mean, if the wavelengths are very different, the smaller one will dominate the value of λ_{d} at most angles.

We consider the behavior of λ_{d} in Fig. 4. It is seen that it approaches λ_{KH} and λ_{RT} at the vertical and horizontal (liquid-above-vapor) configurations, respectively. We also see that there is absolute stability in the region $\alpha < \alpha_{\mathrm{min}}$.

We are now able to make a statement about the range of wavelengths to be expected in a case when going through the possible orientations. The maximum wavelength appearing will be approximately equal to the plate length. The minimum wavelength appearing will be approximately equal to the minimum value of λ_{d}. Since Eq. (66) is not normalized average, it is possible that the minimum wavelength is less than $\min(\lambda_{\mathrm{RT}}, \lambda_{\mathrm{KH}})$, as seen in Fig. 4. In the

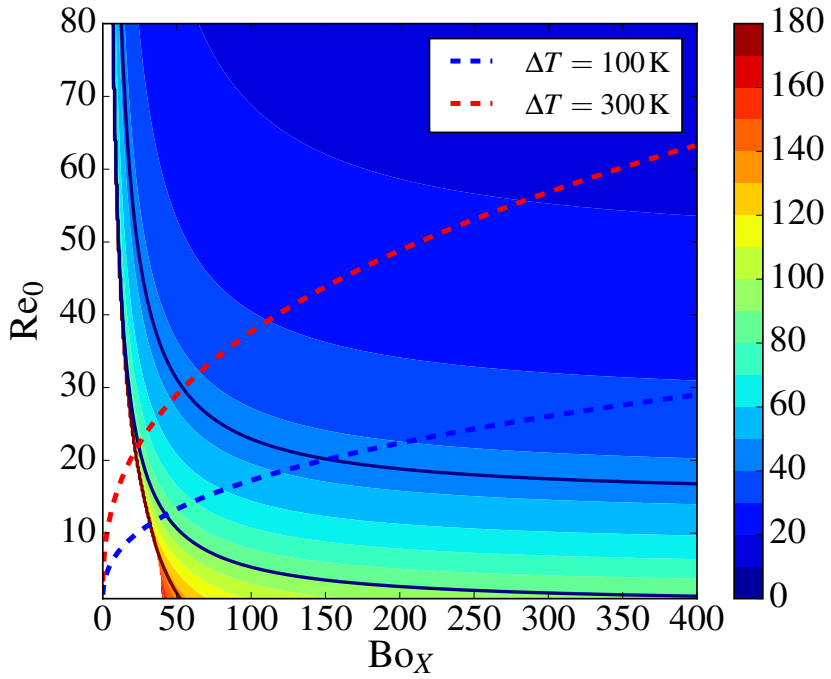

Figure 2: A contour map of α_{crit} (the solution of Eq. (63) as an equality) in degrees across $(\mathrm{Bo}_X, \mathrm{Re}_0)$ space, with $\beta = 10.67$. The white area is the region of global stability. The solid black lines mark specially the angles 45°, 90° and 135°. The dashed lines indicate the domain expected in water film boiling in the region $\Delta T \in (100\,\mathrm{K}, 300\,\mathrm{K})$. Moving to the right along the dashed lines indicate an increased plate length X_0.

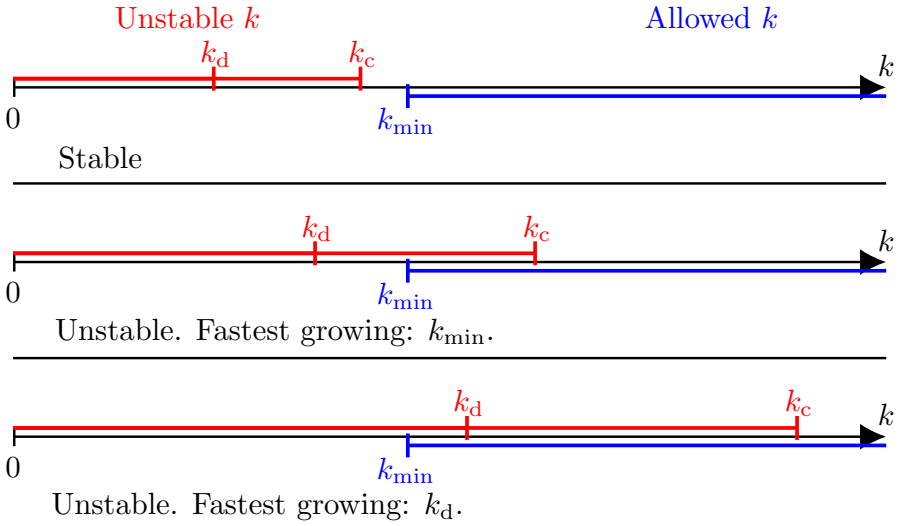

Figure 3: Illustration of the three different states of (in)stability. Top: There is no overlap between unstable wavenumbers and allowed wavenumbers, so the case is stable. Middle: There is overlap between unstable wavenumbers and allowed wavenumbers, so the case is unstable. The wavenumber k_{d} is still not allowed, so the dominant instability will be k_{min}. Bottom: There is overlap between unstable wavenumbers and allowed wavenumbers, so the case is unstable. The wavenumber k_{d} will be the dominant instability.

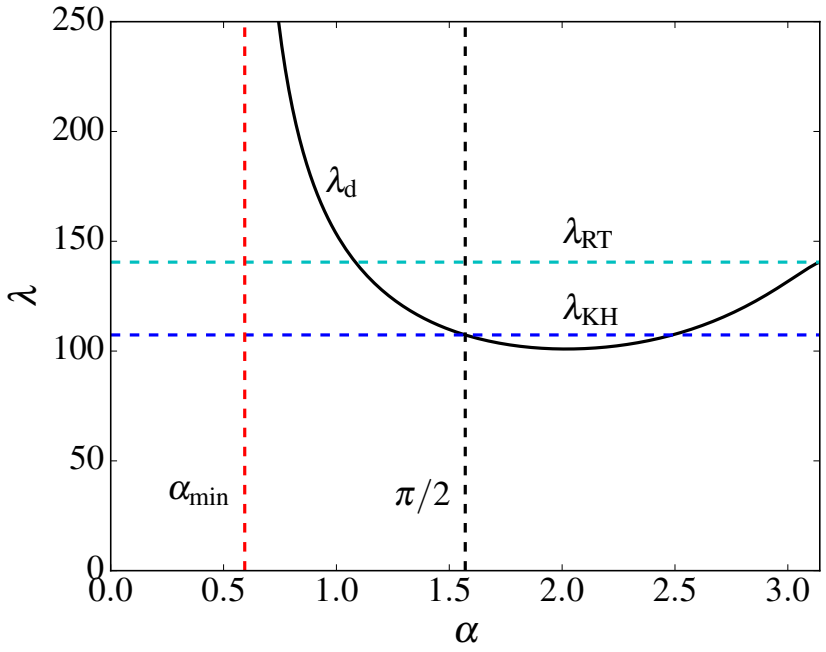

Figure 4: A plot of the fastest growing wavelength according to Eq. (66), with $\mathrm{Bo}_0 = 0.006$ and $\mathrm{We}_0 = 0.013$ (reasonable values for water film boiling), and thus $\mathrm{Re}_0 \approx 23$. Also shown are the limiting wavelengths λ_{RT} and λ_{KH}, according to Eqs. (67) and (68), respectively. The RT wavelength is 30% larger, as predicted by the Reynolds number and Eq. (69).

$a^{5/4} \approx a$ approximation we may solve for this minimum. We find that in the case where one of $(\lambda_{\mathrm{RT}}, \lambda_{\mathrm{KH}})$ is considerably smaller than the other, the minimum wavelength is very close to the smallest of the two. The difference between the minimum wavelength and $\min(\lambda_{\mathrm{RT}}, \lambda_{\mathrm{KH}})$ is largest when the latter two are equal, and in this case the minimum wavelength is about 84% of $\min(\lambda_{\mathrm{RT}}, \lambda_{\mathrm{KH}})$. In summary, we have

$$\begin{aligned} \max(\lambda) &\approx 1/\epsilon_0 \\ \min(\lambda) &\approx \begin{cases} \lambda_{\mathrm{RT}} + \mathcal{O}\left(\Phi_{\mathrm{KH}}^2\right), & \lambda_{\mathrm{RT}} < \lambda_{\mathrm{KH}} \\ \lambda_{\mathrm{KH}} + \mathcal{O}\left((1/\Phi_{\mathrm{KH}})^2\right), & \lambda_{\mathrm{RT}} > \lambda_{\mathrm{KH}} \\ 2^{-1/4}\lambda_{\mathrm{RT}}, & \lambda_{\mathrm{RT}} \approx \lambda_{\mathrm{KH}} \end{cases} \end{aligned} \tag{70}$$

We should now check that the resulting wavelengths satisfy the assumptions of Eq. (56). In terms of wavelength, this can be stated as $2\pi \ll \lambda \ll 2\pi\rho_{\mathrm{l}}/\rho_{\mathrm{v}}$. Since $2\pi\rho_{\mathrm{l}}/\rho_{\mathrm{v}} \approx 10^4$, $\max(\lambda)$ is definitely well below the upper limit. Given the typical range of values indicated in Tab. 2, we get value ranges of $\lambda_{\mathrm{RT}} \in (100, 200)$ and $\lambda_{\mathrm{KH}} \in (40, 400)$. This means that $\min(\lambda)$ is well above the lower limit of 2π.

4.3. Discussion

It is clear from the analysis in Sec. 4.2 that Kelvin–Helmholtz type instabilities are significant in the cases concerned, so much that the critical angle of instability will usually be less than 90° (liquid-below-vapor). At the same time, the stability analysis based on the lubrication approximation PDE, Sec. 4.1 predicts unconditional stability in the vertical and all liquid-below-vapor cases, as its only source of instability is the Rayleigh–Taylor mechanism.

Why does the lubrication approximation fail at capturing the dominant type of instability in cases close to the vertical? The KH instability is an inertial effect, and such effects have been neglected in the lubrication approximation. Formally, terms with both ϵ^2 and $\epsilon\mathrm{Re}$ have been neglected from the Navier–Stokes equation. However, if we have intermediate Re in the range of 10–100, as is the case here, $\epsilon\mathrm{Re}$ may not be so small, and inertial effects may be significant. Remarkably, $\epsilon\mathrm{Re}$ from the steady-state solution in Eq. (28) is independent of both plate length and inclination, and can simply be stated as

$$\epsilon\mathrm{Re} = \frac{4}{3}\frac{Q}{\mu_{\mathrm{v}}}. \tag{71}$$

Thus $\epsilon\mathrm{Re}$ depends only on ΔT and fluid properties. For boiling water with $\Delta T < 200\,\mathrm{K}$, $\epsilon\mathrm{Re} \approx 0.25$, which is still small, but far from negligible. We must have ΔT as low as 80 K to obtain $\epsilon\mathrm{Re} < 0.1$.

Note how the stability criterion Eq. (63) agrees with the sufficient criterion Eq. (49) from the lubrication PDE in the small Re limit. The additional criterion Eq. (50) is not accounted for in the potential flow analysis, since it stems from the source term in the lubrication PDE, and represents stabilization of very thin films through the evaporation effect. In reality, this effect may not be able to stabilize the inertial KH instabilities that are missing from the lubrication model. Here we consider cases with intermediate Re, as shown in Tab. 2, and thus we must prefer the stability analysis of Sec. 4.2.

It is worth pointing out an inconsistency between the origins of the parameter β and how it appears in the potential flow analysis. The attentive reader may notice that the KH term, whose origin is shear, remains nonzero even in the $\beta = 3$ case which represents the case of zero interface shear in the lubrication model. The crucial point here is that only two things are carried over from the lubrication model: The film thickness and the average vapor velocity, both as a function of β. The proper interpretation of β in the context of the potential flow stability analysis is that it shows the effect of the range of possible vapor velocities. However, it does not reflect the actual assumptions behind β in the lubrication model. Instead, the shear in the potential flow stability analysis stems from the given vapor velocity profile and the simplified liquid velocity profile derived in Appendix A. This could in principle be replaced with a more sophisticated model that is consistent with the assumptions behind β in the $\beta \to 3$ limit. However, this was not deemed necessary since the value in real film boiling cases is expected to be much closer to the $\beta \to 12$ limit, in which case the interpretation of β is consistent.

It is interesting to see how the stability criterion Eq. (63) is affected by other factors, at a given plate length and orientation. First of all, it is clear that increased surface tension stabilizes both mechanisms through Bo_X, as expected. For a given surface tension, the KH mechanism's strength is proportional to Re_0. This is given by Eq. (34), showing the dependency $\sim Q^{3/4}$. Thus a smaller superheat ΔT will decrease the Reynolds number, through decreasing both h_0 and u_0. This creates somewhat of a paradox, as we predict a very thin but very stable vapor film as $\Delta T \to 0$ in the vertical case, while from reality it is known that film boiling must break down at some finite ΔT (vapor film collapse at the Leidenfrost point (Dhir, 1998)). This can possibly be resolved by introducing additional mechanisms of instability that become pronounced at very small film thicknesses, such as van der Waals and thermo-capillary effects.

Finally, it should be recognized that the final stability criterion Eq. (63) is obtained through potential flow stability analysis applied to a steady state derived under the assumption that viscous forces dominate. Therefore the results herein must mainly be interpreted qualitatively, or quantitatively as a rough approximation.

5. Example case

In order to illuminate the results, we consider the example of water film boiling at atmospheric pressure. Additional case parameters to vary are then the superheat ΔT and the plate length X_0. We vary these in the region 100–250 K and 1–5 cm, respectively. This gives steady-state film thickness scales of $h_0 \approx 130$–$250\,\mu\mathrm{m}$.

We may again investigate α_{crit}, the first angle where the inequality Eq. (63) is broken and instabilities arise. The results are shown in Fig. 5. We see that the possibility of $\pi/2 < \alpha_{\mathrm{crit}} < \pi$ is very rare: Either instabilities arise while still in the liquid-below-vapor configuration, or they never arise at all (global stability). This means that in most cases, the initial instabilities arising when rotating the plate will be caused purely by KH instabilities, not RT instabilities. We also see that the sensitivity due to degree of superheat is quite small.

We may also choose a specific plate length, in this case $X_0 = 5\,\mathrm{cm}$, and investigate how the dimensional fastest growing wavelength $\tilde{\lambda}_{\mathrm{d}}$ depends on the inclination angle. Here we get Reynolds numbers in the range $\mathrm{Re}_0 \in (40, 60)$, and thus $\Phi_{\mathrm{KH}} \in (3, 5)$. This means that the KH effect will dominate at most orientations, and also that λ_{KH} (found at $\alpha = 90°$) is less than λ_{RT} (found at $\alpha = 180°$), as shown in Fig. 6. We again observe a relatively weak dependence on superheat, with all cases giving wavelengths in the range 1–5 cm. We see that when $\alpha \to \pi$ we approach a single RT wavelength, as $\tilde{\lambda}_{\mathrm{RT}}$ only depends on the (assumed constant) fluid thermo-physical properties.

6. Experimental comparison

Unfortunately there are few experimental works studying the influence of inclination on film boiling stability. However, one such study was published by Kim and Suh (2013), which included indirect approximate measurements of the maximum stable film thickness for water film boiling. The principle behind the measurements is as follows: A planar film boiling experiment is performed with a plate much longer than the characteristic wavelengths of instability. They then assume that the film grows according to the smooth steady-state solution until its limit of stability. The film then collapses, and begins growing again from a very small thickness, thus forming a repeating pattern. Given the approximations that the collapse happens very rapidly, and resets the film to a thickness of practically zero, steady solutions of the form $\sim x^{1/4}$ will give the property that

$$\mathrm{HTC} \approx \frac{4k_{\mathrm{v}}}{3h_{\max}}, \tag{72}$$

where HTC is the average heat transfer coefficient over the long plate, and $h_{\max}$ is the peak film thickness right before the reset. The authors measured HTC, thus providing indirect measurement for $h_{\max}$. This was performed with a range of α and ΔT values.

From the present model, we may attempt to predict $h_{\max}$ by searching for the first point where k_{d} becomes an allowable wavenumber, i.e. numerically solve

$$k_{\mathrm{d}}(x_0) = k_{\min}(x_0) \tag{73}$$

for x_0, while using Eq. (65) for k_{d}. This is similar to what was done by Kolev (1998), except that due to the vertical orientation, purely Kelvin–Helmholtz wavelengths were considered. Once the solution has been found, Eq. (28) can be used as a predictor for $h_{\max}$. The vapor properties should in each case be set according to the average film

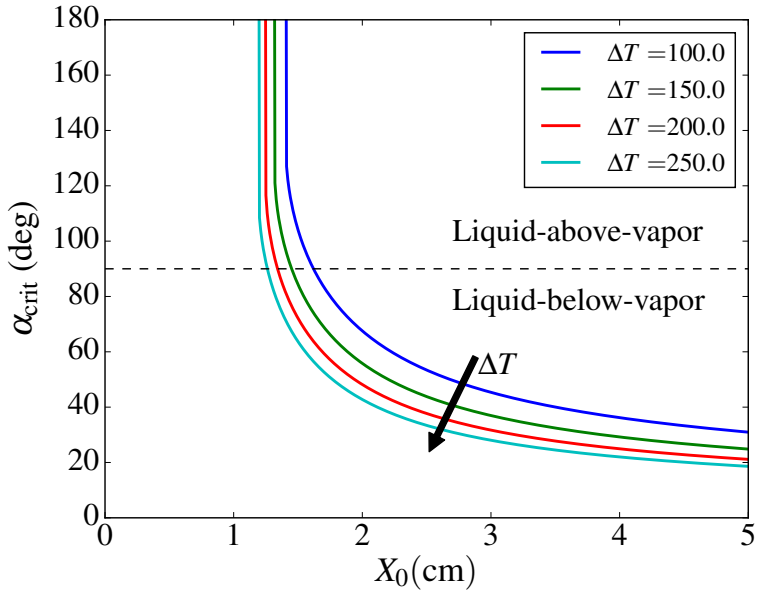

Figure 5: Critical inclination angle for loss of stability plotted against plate length, according to Eq. (63), for various degrees of superheat.

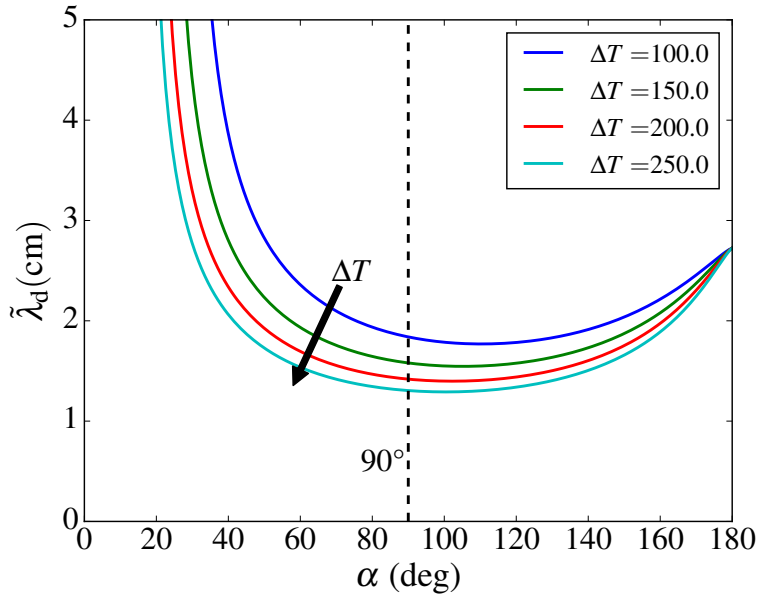

Figure 6: Dimensional fastest growing wavelength, $\tilde{\lambda}_{\rm d} = h_0 \lambda_{\rm d}$ according to Eq. (66), plotted against inclination angle, for various degrees of superheat. The plate length is $X_0 = 5\,$cm.

temperature. A comparison with the experimental values for $h_{\max}$ is shown in Fig. 7 as a function of inclination angle α. The experiments were run with ΔT in the region 100–200 K. However, this parameter was not strictly controlled and has only a small effect on $h_{\max}$, so these points were simply grouped together at their α values. The model predictions were calculated for the edges of this ΔT range, and plotted as a band of possible values.

The comparison in Fig. 7 is quite close and qualitatively similar. It can never be expected to be a perfect prediction, for two reasons. First, the measurement of $h_{\max}$ is indirect, and the conversion from the actual measured quantity, HTC, is dependent on approximations and assumptions. Second, what is being measured is not a property of a small (linear) wave disturbance, but rather an averaged property of a fully developed instability. Thus the stability analysis in the present work can only be expected to be an approximate predictor. In that respect, it appears successful.

Note that the prediction has zero fitted or empirical parameters, as the value of β is calculated from fluid properties through Eq. (A.6) in Appendix A. In contrast, the model in Kim and Suh (2013) is dependent on fitting two parameters to the experiments. Note also how the stability analysis of the lubrication PDE in Sec. 4.1 predicts unconditional stability throughout the entire range of $\alpha \in [0, \pi/2]$ in Fig. 7, and thus the corresponding predicted $h_{\max}$ would be infinite. We therefore see that including Kelvin–Helmholtz effects is crucial.

7. Conclusions

From the model analyses and examples in this work, we may draw the following conclusions:

- In planar vertical or inclined film boiling, parallel velocities can become large enough to make Kelvin-Helmholtz type instabilities important.
- The transient model Eq. (43) based on the lubrication approximation is not capable of predicting these Kelvin-Helmholtz type instabilities, only Rayleigh-Taylor type instabilities. It will thus incorrectly predict absolute stability in e.g. the vertical case.
- When applying classical potential flow stability analysis to the steady-state solution of the lubrication model, both types of instabilities can be predicted.
- We identified an angle $\alpha_{\min}$, given by Eq. (64), below which there will be stability regardless of surface tension. This angle depends on the vertical case Reynolds number Re_0.
- The full stability criterion, including surface tension stabilization, is given by Eq. (63). This allows the numerical calculation of α_{crit}, the angle of instability onset. We saw from Fig. 2 that in most cases, instabilities arise before reaching the vertical configuration, i.e. in the liquid-below-vapor configurations. In these cases, instabilities are purely due to Kelvin-Helmholtz effects.
- Once well into the unstable region, the characteristic wavelength of the instabilities will be an inclination-dependent harmonic mean like combination of the Rayleigh–Taylor and Kelvin–Helmholtz wavelengths, as given by Eq. (66). Due to the way vapor velocity and film thickness develop in film boiling, the two wavelength contributions turn out to be quite similar, as shown in Eq. (69). The range of wavelengths possible when passing through all orientations is summed up in Eq. (70).
- From the practical case of water film boiling in Sec. 5, we saw that the critical angle and characteristic wavelengths are only weakly dependent on the degree of superheat. Depending on plate length, most cases will either be globally stable, or have $\alpha_{\mathrm{crit}} < 45°$, with only a small intermediate region. The case had Kelvin–Helmholtz wavelengths in the range of 1–2 cm, depending on superheat, while the Rayleigh–Taylor wavelengths were 2.7 cm.
- We saw that the model is reasonably able to predict how the limit of stability depends on inclination, based on experimental data from the literature.

The second point does not mean that the standard lubrication approximation is useless for describing film boiling in general. However, it does mean that it is likely incapable of correctly describing transient dynamics of inclined or vertical film boiling. Using the lubrication approximation to predict dynamics in horizontal film boiling, such as in Panzarella et al. (2000) and Kim et al. (2015) is still valid, as these cases do not have significant shear/inertial forces.

While the stability criterion derived herein may be somewhat successful at predicting the onset of instabilities, it is not sufficient for simulating the full nonlinear behavior of the vapor film as the instabilities grow. Doing this would require a PDE such as Eq. (43), but as we have shown, this model cannot predict the onset of the Kelvin–Helmholtz type instabilities. In further work, if one still wants to avoid solving the full set of governing equations and boundary conditions, the thin-film model derivation of Sec. 2 may have to be mended to include inertial terms to leading order. This may be possible through Karman–Pohlhausen methods (Dávalos-Orozco et al., 1997), as demonstrated for a vertically falling liquid film by Alekseenko et al. (1985). Also, if one also wants to predict vapor film collapse at lower superheat values, it may be necessary to include additional instability mechanisms such as van der Waals forces and thermo-capillary effects (Burelbach et al., 1988; Oron et al., 1997). Including the latter would necessitate using a non-equilibrium evaporation model, to allow for tangential interface temperature gradients.

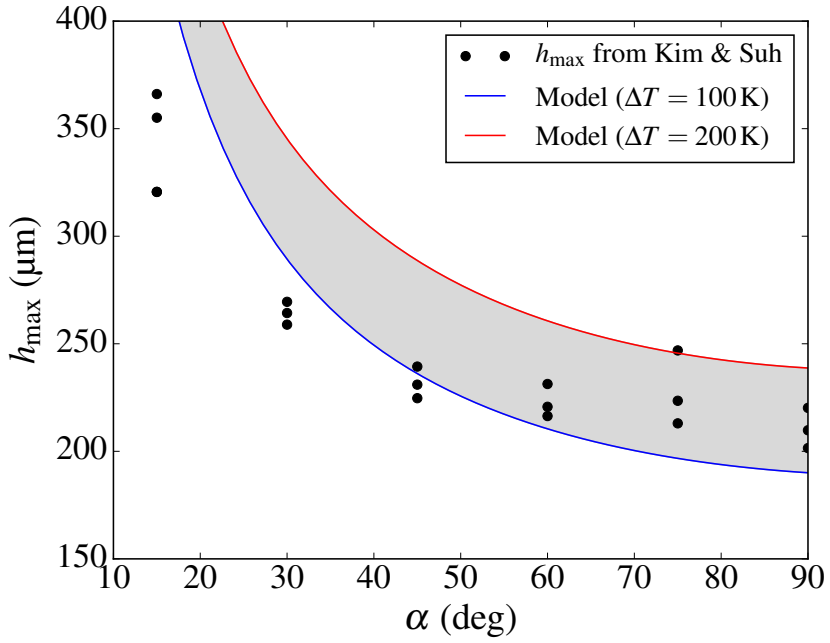

Figure 7: A comparison of the angular dependence of $h_{\max}$ from Kim and Suh (2013) with predictions using the present model. The gray band shows the range of predictions for the same range of ΔT values as the experiments.

Appendix A. Liquid velocity profile

In Sec. 2.1, we avoided having to calculate the liquid flow outside of the vapor film by introducing the factor β, which has the values 3 or 12 in the two possible extreme cases. The former comes from assuming that the liquid applies no shear stress on the vapor (free surface), while the latter comes from assuming a zero tangential liquid velocity. The actual value of β, and thus the actual mass flow rate from Eq. (7), must be somewhere in between. In this section we attempt to approximate this value from the viscosity ratio of the liquid–vapor pair. First we make the assumption of a reciprocal liquid velocity profile

$$u_{\mathrm{l}}(z) = \frac{C}{z}, \tag{A.1}$$

where C is some constant to be found. This is arguably ad-hoc, but retains the desired property of both u_{l} and $\partial u_{\mathrm{l}}/\partial z$ going to zero as $z \to \infty$. The boundary conditions at the liquid–vapor interface give the vapor velocity profile

$$u(z) = \frac{Dh^2}{2\mu_{\mathrm{v}}}\left[\left(\frac{\Psi+2}{\Psi+1}\right)\frac{z}{h} - \left(\frac{z}{h}\right)^2\right], \tag{A.2}$$

and the liquid velocity profile

$$u_{\mathrm{l}}(z) = \frac{Dh^2}{2\mu_{\mathrm{v}}}\frac{1}{(\Psi+1)}\frac{h}{z}, \tag{A.3}$$

where we have defined the viscosity ratio

$$\Psi = \frac{\mu_{\mathrm{l}}}{\mu_{\mathrm{v}}}. \tag{A.4}$$

The average vapor velocity is then

$$\bar{u} = \frac{Dh^2}{12\mu_{\mathrm{v}}}\frac{\Psi+4}{\Psi+1}, \tag{A.5}$$

which may be compared with the average velocity implied by Eq. (7) to give the relation

$$\beta = 12\frac{\Psi+1}{\Psi+4}. \tag{A.6}$$

We see that the limit $\Psi \to \infty$ corresponds to $\beta = 12$, and that the limit $\Psi \to 0$ corresponds to $\beta = 3$. The viscosity ratio Ψ at saturation for either water or cryogens is typically in the range 20–30. For values that large, Eq. (A.6) is not very sensitive to Ψ, and this range of Ψ gives the narrow range of $\beta = 10.75 \pm 0.25$. We see that this is quite close to the assumption of zero interface velocity ($\beta = 12$). Specifically for boiling water, the value is $\beta = 10.67$.

The value of β (or Ψ) decides the ratio between the interface velocity and the average vapor velocity, and this can be found as

$$\frac{u_{\mathrm{i}}}{\bar{u}} = \frac{6}{\Psi+4} = \frac{1}{6}(12-\beta). \tag{A.7}$$

Note that the rightmost expression in Eq. (A.7) (in terms of β) does not actually require the assumption of a particular velocity profile, as long as we can assume that $u_{\mathrm{i}}/\bar{u}$ should be a linear function of β between the well defined extremes $\beta = 3$ and $\beta = 12$.

Acknowledgments

This publication is based on results from the research project *Predicting the risk of rapid phase-transition events in LNG*

spills (Predict-RPT), performed under the MAROFF program. The authors acknowledge the Research Council of Norway (244076/O80) for support. Special thanks to Tor Ytrehus, Bernhard Müller, Svend Tollak Munkejord, and Morten Hammer for fruitful discussions and feedback.

References

S. V Alekseenko, V. E. Nakoryakov, and B. G. Pokusaev. Wave formation on vertical falling liquid films. *International journal of multiphase flow*, 11(5):607–627, 1985. doi:10.1016/0301-9322(85)90082-5.

E Aursand. Modelling planar film boiling of arbitrary inclination with the lubrication approximation. In B. Skallerud and H. I. Andersson, editors, *Proceedings of the 9. National Conference on Computational Mechanics MekIT'17*. CIMNE, 2017.

G. Berthoud. Vapor explosions. *Annual Review of Fluid Mechanics*, 32(1):573–611, 2000. doi:10.1146/annurev.fluid.32.1.573.

L. A. Bromley. Heat transfer in stable film boiling. *Chemical Engineering Progress*, 46:221–227, 1950.

T. D. Bui and V. K. Dhir. Film boiling heat transfer on an isothermal vertical surface. *ASME J. Heat Transfer*, 107(4):764–771, 1985. doi:10.1115/1.3247502.

J. P. Burelbach, S. G. Bankoff, and S. H. Davis. Nonlinear stability of evaporating/condensing liquid films. *Journal of Fluid Mechanics*, 195:463–494, 1988. doi:10.1017/S0022112088002484.

P. Cleaver, M. Johnson, and B. Ho. A summary of some experimental data on LNG safety. *Journal of Hazardous Materials*, 140(3):429–438, 2007. doi:10.1016/j.jhazmat.2006.10.047.

R. V. Craster and O. K. Matar. Dynamics and stability of thin liquid films. *Reviews of modern physics*, 81(3):1131–1198, 2009. doi:10.1103/RevModPhys.81.1131.

L. A. Dávalos-Orozco, S. H. Davis, and S.G. Bankoff. Nonlinear instability of a fluid layer flowing down a vertical wallunder imposed time-periodic perturbations. *Physical Review E*, 55(1):374–380, 1997. doi:10.1103/PhysRevE.55.374.

V. K. Dhir. Boiling heat transfer. *Annual review of fluid mechanics*, 30(1):365–401, 1998. doi:10.1146/annurev.fluid.30.1.365.

P. G. Drazin and W. H. Reid. *Hydrodynamic stability*. Cambridge University Press, Cambridge, 2nd edition, 2004. ISBN 9780631525417.

D. F. Fletcher. Steam explosion triggering: a review of theoretical and experimental investigations. *Nuclear Engineering and Design*, 155:27 – 36, 1995. doi:10.1016/0029-5493(94)00865-V.

D.W. Hissong. Keys to modeling LNG spills on water. *Journal of Hazardous Materials*, 140(3):465 – 477, 2007. doi:10.1016/j.jhazmat.2006.10.040.

S. W. Joo, S. H. Davis, and S. G. Bankoff. Long-wave instabilities of heated falling films: two-dimensional theory of uniform layers. *Journal of Fluid Mechanics*, 230:117–146, 1991. doi:10.1017/S0022112091000733.

H. Jouhara and B. P. Axcell. Film boiling heat transfer and vapour film collapse on spheres, cylinders and plane surfaces. *Nuclear Engineering and Design*, 239(10):1885–1900, 2009. doi:10.1016/j.nucengdes.2009.04.008.

H.I. Jouhara and B.P. Axcell. Forced convection film boiling on spherical and plane geometries. *Chemical Engineering Research and Design*, 80(3):284–289, 2002. doi:10.1205/026387602753582060.

B. J. Kim and K. D. Kim. Rayleigh-taylor instability of viscous fluids with phase change. *Physical Review E*, 93(4):043123, 2016. doi:10.1103/PhysRevE.93.043123.

B. J. Kim, J. H. Lee, and K. D. Kim. Rayleigh–taylor instability for thin viscous gas films: Application to critical heat flux and minimum film boiling. *International Journal of Heat and Mass Transfer*, 80:150–158, 2015. doi:10.1016/j.ijheatmasstransfer.2014.08.084.

C. S. Kim and K. Y. Suh. Angular dependency on film boiling heat transfer from relatively long inclined flat plates. *Journal of Heat Transfer*, 135(12):121502, 2013. doi:10.1115/1.4024583.

J. C. Y. Koh. Analysis of film boiling on vertical surfaces. *Journal of Heat Transfer*, 84(1):55–62, 1962. doi:10.1115/1.3684293.

N. I. Kolev. Film boiling on vertical plates and spheres. *Experimental Thermal and Fluid Science*, 18(2):97–115, 1998. doi:10.1016/S0894-1777(98)10021-3.

P. K. Kundu, I. M. Cohen, and D. R. Dowling. *Fluid Mechanics*. Academic Press, Cambridge, 5th edition, 2007. ISBN 9780123821003.

A. Luketa-Hanlin. A review of large-scale LNG spills: Experiments and modeling. *Journal of Hazardous Materials*, 132:119 – 140, 2006. doi:10.1016/j.jhazmat.2005.10.008.

T. G. Myers. Thin films with high surface tension. *SIAM Review*, 40(3):441–462, 1998. doi:10.1137/S003614459529284X.

S. Nishio and G. R. Chandratilleke. Natural-convection film-boiling heat transfer: Saturated film boiling with long vapor film. *JSME international journal. Ser. 2, Fluids engineering, heat transfer, power, combustion, thermophysical properties*, 34(2):202–211, 1991. doi:10.1299/jsmeb1988.34.2_202.

S. Nukiyama. The maximum and minimum values of the heat Q transmitted from metal to boiling water under atmospheric pressure. *Journal of Japan Society of Mechanical Engineers*, 37:367–374, 1934.

A. Oron, S. H. Davis, and S. G. Bankoff. Long-scale evolution of thin liquid films. *Reviews of modern physics*, 69(3):931–980, 1997. doi:10.1103/RevModPhys.69.931.

C. H. Panzarella, S. H. Davis, and S. G. Bankoff. Nonlinear dynamics in horizontal film boiling. *Journal of Fluid Mechanics*, 402:163–194, 2000. doi:10.1017/S0022112099006801.